Inorganic Chemistry

Article

pubs.acs.org/IC

Enhanced Anode Performances of Polyaniline–TiO_2–Reduced Graphene Oxide Nanocomposites for Lithium Ion Batteries

Fan Zhang,[†,‡] Huaqiang Cao,*[,‡] Dongmei Yue,*[,†] Jingxian Zhang,[§] and Meizhen Qu[§]

[†]College of Materials Science and Engineering, Beijing University of Chemical Technology, Beijing 100029, P. R. China

[‡]Department of Chemistry, Tsinghua University, Beijing 100084, P. R. China.

[§]Chengdu Institute of Organic Chemistry, Chinese Academy of Sciences, Chengdu 610041, P. R. China

Supporting Information

ABSTRACT: Here, we report a three-layer-structured hybrid nanostructure consisting of transition metal oxide TiO_2 nanoparticles sandwiched between carbonaceous polymer polyaniline (PANI) and graphene nanosheets (termed as PTG), which, by simultaneously hindering the agglomeration of TiO_2 nanoparticles and enhancing the conductivity of PTG electrode, enables fast discharge and charge. It was demonstrated that the PTG exhibited improved electrochemical performance compared to pure TiO_2. As a result, PTG nanocomposite is a promising anode material for highly efficient lithium ion batteries (LIBs) with fast charge/discharge rate and high enhanced cycling performance [discharge capacity of 149.8 mAh/g accompanying Coulombic efficiency of 99.19% at a current density of 5C (1000 mA/g) after 100 cycles] compared to pure TiO_2. We can conclude that the concept of applying three-layer-structured graphene-based nanocomposite to electrode in LIBs may open a new area of research for the development of practical transition-metal oxide graphene-based electrodes which will be important to the progress of the LIBs science and technology.

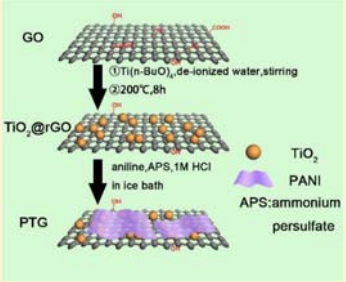

1. INTRODUCTION

Rechargeable lithium ion batteries (LIBs) are an attractive power source for applications in portable electronic devices and electric and hybrid vehicles.[1] Good electrode materials imply high energy density, long cycle life, and excellent rate capability performance, and therefore, high reversible storage capacity for Li^+ and rapid Li^+ transport. However, it is still a major challenge to develop a new concept to construct electrode materials with rapid charge and discharge rates in LIBs,[2] besides high-capacity LIBs.[3] To achieve this goal, there has been an intensive search for new electrode materials with a promising rate capability performance for use as anodes. It is well-known that nanomaterials used in LIBs can circumvent the electrode kinetic issues,[1b] which would reduce the lithium diffusion time that accompanies the Faradaic reactions of active particles, due to the short ion and electron transport pathways. Another advantage of nanostructured electrode materials is better accommodation of the strain of lithium insertion/extraction, thus improving cycle life. However, nanoparticle agglomeration and dissolution during the discharge/charge cycling processes will lead to reduction of electroactive sites and degradation of reversible performance. Thus, it is necessary to avoid nanoparticle agglomeration during cycling processes.

Among the transition-metal oxides, nanostructured TiO_2 has been widely investigated as a key material for fundamental research and technological applications in the fields of photovoltaic devices,[4] semiconductor solar cells,[5] and catalysts.[6] Especially, much interest has been aroused in nanostructured TiO_2 for application in LIBs as a fast lithium insertion/removal.[7] It is regarded that the anatase phase of TiO_2, being abundant, low-cost, environment-friendly, and nontoxic, is the most electroactive lithium-insertion host as far as TiO_2 is concerned. There are nearly no lattice changes during Li^+ insertion/extraction processes in TiO_2-based structures, which can enhance structural stability and prolong the cycle life.[8] However, the charge/discharge rates of bulk TiO_2 material will be greatly limited due to the poor ionic and electronic conductivity. In order to achieve a high rate capacity of LIBs, rapid lithium ion and electron diffusions are necessary, which can be resolved by doping conductive phases in TiO_2. It has been demonstrated that carbonaceous interpenetrating structures can be fabricated to serve as conductive pathways in LIBs.[2a] Conducting polyaniline (PANI), compared with other conducting polymers, is advantageous for easy synthesis, low cost, physical properties controlled by both oxidation and protonation state, and easy fabrication in the form of films grafted onto the surface of metallic or semiconductor electrodes by chemical methods, and has been used as electrode materials in rechargeable batteries.[9]

It has aroused our great interest to develop new oxide-based nanocompositions as anode materials in LIBs,[2c,10] such as Fe_3O_4-,[10a,b] Co_3O_4-,[10c] and SnO_2-based,[10d,e] as well as TiO_2-based[2c] nanocomposites. However, most[10] of them are focused on improving the capacity and cycleability, and not on fast charging/discharging properties of anode materials in LIBs, except the TiO_2-reduced graphene oxide composite (TGC) hybrid nanocomposite in which TiO_2 has fast Li insertion/

Received: June 27, 2012
Published: August 20, 2012

   dx.doi.org/10.1021/ic301378j | Inorg. Chem. 2012, 51, 9544–9551

extraction host properties.[2c] The TGC presents high rate capability which is attributed to the transport advantages of the unique structure of TGC, such as short transport paths as well as high electrode−electrolyte contact area.[2c]

Recently, we successfully introduced PANI into graphene-based SnO_2 hybrid materials (SPG) used as an anode material in LIBs which presents enhanced electrochemical behavior compared with previously reported SnO_2.[10e] This result is attributed to the novel structure of SPG: (i) the pulverization problem caused by the formation of Sn nanoparticles during the charge/discharge processes can be reduced; (ii) the formed Sn nanoparticles will attach on the surface of the PANI-rGO layers, which is favorable to the electron and lithium ion transfer; and (iii) SnO_2 nanoparticles can provide a short diffusion length for Li^+ insetion.[10e] It is known that there is a severe pulverization problem for SnO_2-based materials to overcome the extremely large volume change of 311% produced by the alloying reaction between Sn and Li during Li^+ insertion process to form $Li_{4.4}Sn$.[11] So we synthesized SPG by applying a two step process: the synthesis of polyaniline (PANI)@graphene oxide (GO) which can form various spacing on the surface of GO. This spacing will be favorable to release the great strain generated in Li^+ insertion process. Then, we anchored SnO_2 on the PANI@GO sheets and embedded in the spaces between the PANI nanosheets, and simultaneously reducted GO into rGO, leading to the formation of SnO_2@PANI@rGO. However, there is only a neglectable volume change (<4%) for TiO_2 as anode in LIBs.[2c,12] The pulverization problem is not a key issue for TiO_2-based anode materials, but the enhancing charge/discharge rate for TiO_2-based anode materials in LIBs becomes a key issue. Because of the low conductivity ($\sim 10^{-13}$ S/cm) of TiO_2, it will limit its application for high power outputs.[12]

Rapid charging/discharging rates have become a key issue for LIBs, despite the observation that this can lead to prominent reductions in the capacity.[2a] Herein, we report a transition metal oxide sandwiched nanocomposite concept consisting of TiO_2 nanoparticles sandwiched between conducting polymer PANI films and graphene nanosheets (termed as PTG) (Scheme 1), which, by simultaneously hindering the agglomeration of TiO_2 nanoparticles and enhancing the conductivity of TiO_2 electrode by doping PANI and graphene nanosheets[10a] in the TiO_2-based nanocomposites, enables fast discharge and charge rates.

Scheme 1. Synthesis Steps and Structure of Anatase Polyaniline-TiO_2-Reduced Graphene Oxide (PTG) Nanocomposites

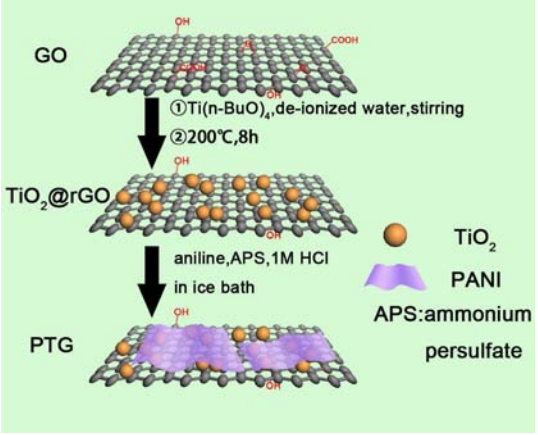

2. EXPERIMENTAL SECTION

2.1. Synthesis of TiO_2@rGO. The graphene oxide (GO) sheets used in this work were prepared using a modified Hummer's method.[10a] A 200 mg GO sample was dispersed in 200 mL of deionized water by stirring for 10 min, followed by ultrasonic treatment for 2 h. A tetra-n-butyltitanate (chemically pure, CP, ≥ 98%, Sinopharm Chemical Reagent Co., Ltd., 3825 mg) solution was prepared by dissolving in 100 mL of alcohol, followed by adding this solution into the above GO solution under stirring for 10 min. Then, the solid product was collected by suction filtration of the solution, followed by washing with deionized water for three times. After the heat treatment at 200 °C for 8 h, TiO_2@reduced graphene oxide (rGO) was obtained.

2.2. Synthesis of PANI-TiO_2@RGO (PTG). The TiO_2@rGO product was ground into powder, and then was dispersed in 100 mL of deionized water for 10 min, followed by consecutively adding 0.2 mL of aniline (analytical reagent, AR, ≥99.5%, Guangdong Xilong Chemical Co., Ltd.) and 80 mL of HCl (1 M) with stirring for 15 min to generate solution A. Ammonium persulfate (980.12 mg, AR, ≥98%, Guangdong Xilong Chemical Co., Ltd.) was dissolved in deionized water (50 mL) to generate solution B. Solution A was placed under ice bath conditions with stirring, followed by adding solution B with stirring overnight. After washing and drying naturally, PANI-TiO_2@RGO (termed as PTG) was obtained.

2.3. Synthesis of TiO_2 Nanoparticles. The TiO_2 nanoparticles were synthesized by using the similar process of TiO_2@rGO without adding GO in the reaction system.

2.4. Characterization. The phase structure was studied by X-ray diffractometer (Druker D8 Advance) with Cu Kα radiation (λ = 1.5406 Å, operating at 40 kV × 40 mA). Fourier transform infrared (FT-IR) spectrum measurement was carried out on a NICOLET 560 and NICOLET 6700 Fourier transform infrared spectrophotometer. Resonance Raman spectra were recorded on a Renishaw RM 1000 with excitation from the 514.5 nm line of an Ar-ion laser with a power of 5 mW at room temperature. X-ray photoelectron spectra (XPS) were obtained by a PHI quantera SXM with an Al Kα = 280.00 eV excitation source, where binding energies were calibrated by referencing the C1s peak (284.8 eV) to reduce the sample charge effect. The morphology was studied by transmission electron microscopy (TEM, Hitachi H-7650B, operating at 80.0 kV). Atomic force microscopy (AFM) measurement was carried out on a Digital Instruments Dimension 3100 microscope with a NanoScope IIIa control unit in the tapping mode. Adsorption−desorption isotherms of nitrogen at 77 K were recorded on TriStar II 3020 equipment (Micromeritics Instrument Corporation, USA).

2.5. Lithium Ion Battery Performance Measurements. Electrochemical charge and discharge tests were made in CR 2032 type coin cells assembled in an argon-filled glovebox (MBRAUN). The working electrodes prepared by mixing the as-synthesized sample and carboxymethyl cellulose sodium (CMC, 3 wt %) at a weight ratio of 90:10 were pasted on pure Cu foil (15 μm). Celgard 2400 was used as a separator. Lithium foil was used as the counter electrode. The electrolyte consisted of a solution of $LiPF_6$ (1 M) containing vinylene carbonate (2%) in ethylene carbonate/dimethyl carbonate/diethyl carbonate (1:1:1, volume ratio). The electrochemical performances were evaluated by using a BS-9300 system (Guangzhou Kinte Industrial Co., Ltd.) under room temperature. The coin cells were discharged and charged between 0.01 and 2.5 V (vs Li^+/Li) at current density of 0.2 C, 0.5 C, 1 C (1 C = 200 mA/g), 2 C, 5 C, and 10 C, respectively. The weight of as-synthesized PTG sample in the working electrode was used to estimate the specific discharge capacity of the LIBs, which was expressed in mAh/g of PTG. The TiO_2 anode was prepared with a similar process and the same loading mass as that of PTG anodes in LIBs.

2.6. Cyclic Voltammetry Measurements. The cyclic voltammetry (CV) measurement was studied by a CHI 660B electrochemical

dx.doi.org/10.1021/ic301378j | Inorg. Chem. 2012, 51, 9544−9551

analyzer interfaced to a computer system with corresponding electrochemical software. The electrode (2.0 cm × 4.0 cm) was loaded with 5 mg PTG or pure TiO_2 wrapped in foam nickel plate prepared under 10−12 MPa as counter electrode and working electrode and tested in the potential range −0.1−0.4 V, with AgCl/Ag in saturated KCl solution used as a reference electrode, and 6 M KOH solution as the supporting electrolyte. The CV response of the electrodes was measured at different sweep rates varying from 5 to 100 mV/s.

3. RESULTS AND ANALYSIS

The XRD pattern (Figure 1) of the as-synthesized sample of PTG demonstrates that the TiO_2 belongs to anatase TiO_2

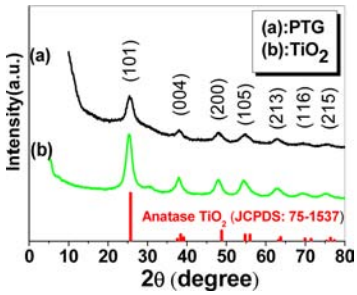

Figure 1. XRD patterns of (a) PTG and (b) TiO_2.

(JCPDS card 75-1537). Usually, the XRD pattern of GO will show a typical (002) peak located at 12.4°, corresponding to an interlayer spacing of 0.776 nm. However, we cannot observe the sharp peak around 12.4° in the XRD pattern of PTG, suggesting that GO has been reduced to rGO via the thermal reduction mechanism of changing GO into rGO. No peaks for graphite [26.6°, (002)] can be observed, suggesting no further agglomeration of few-layer rGO sheets which were hindered by TiO_2 nanoparticles.[10a] This will be further demonstrated by Raman data. The averaged TiO_2 particle size is about 4.7 nm according to the (101) peak reflection using the Scherrer equation,[13] which is well consistent with TEM observation. The averaged size of pure TiO_2 nanoparticles is about 4.7 nm, corresponding to the TEM observation (Figure S1).

The Fourier transform infrared (FT-IR) spectrum of the PTG is shown in Figure 2a. The absorption signals in the range

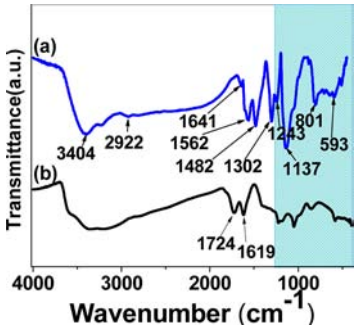

Figure 2. FT-IR spectra of (a) PTG and (b) GO.

400−1250 cm^{-1} are characteristic of the formation of O−Ti−O lattice.[14] The broad peak centered at 3404 cm^{-1} is attributed to N−H stretching mode.[15] The weak peak at 2922 cm^{-1} is attributed to Ar−H stretching vibration.[15] A very low intensity peak centered at 1641 cm^{-1} is attributed to an O—H bending vibration, due to the adsorbed H_2O.[14] A strong peak at 1562 cm^{-1} is attributed to C═C in benzenoid rings.[15] The peak at 1482 cm^{-1} is attributed to bending mode of N—H.[15] The peak at 1302 cm^{-1} is attributed to C−N stretching mode of aryl carbon.[16] These data demonstrated that the TiO_2 and polyaniline coexist in PTG. As a control, we provided the GO spectrum in Figure 2. The stretching vibrations of carboxyl groups (1724 cm^{-1}) and antisymmetric stretching vibration of COO^- (1619 cm^{-1}) as well as a broad O−H stretching vibration at 3100−3600 cm^{-1} cannot be observed in PTG but presented in GO (Figure 2b),[16] which means the reduction of GO to rGO is completed by the thermal treatment process.

Figure 3 shows the Raman spectra of PTG and GO. The peaks at 120, 412, 532, 620, and 812 cm^{-1} are attributed to

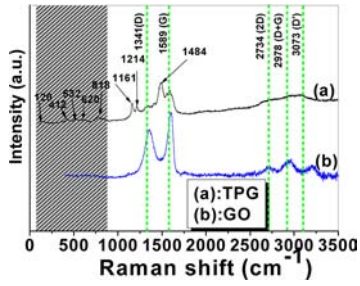

Figure 3. Raman spectra of (a) PTG and (b) GO.

Raman modes of $E_g(1)$, $B_{1g}(1)$, A_{1g}, $E_g(3)$, and the first overtone of B_{1g} of anatase phase of TiO_2, respectively.[17] The first E_g peak at 120 cm^{-1} is obviously shifted with respect to that of bulk TiO_2 crystal at 142 cm^{-1} on the basis of the space-theoretical analysis.[17] It is known that several properties do not differ from those of the bulk unless the dimension is less than the typical 20 nm.[18] The Raman spectra present marked asymmetry toward the low-wavenumber side when the particle size reduces, on the basis of the Gaussian confinement model of optical phonon confinement effect.[19] The first E_g mode is influenced by the grain size of the TiO_2 nanocrystals which presents a shift toward the low-wavenumber side compared with that of bulk TiO_2 due to its small size of 4.7 nm, below a typical size of 20 nm. The Raman peaks at 1161, 1214, 1484, and 1580 cm^{-1} are associated with the following vibrational modes: C—H benzenoid or quinoid stretching vibration, C—N benzenoid stretching vibration, C═N quinoid stretching vibration, and C═C stretching vibration, respectively, due to the polyaniline molecules.[20] The Raman peaks at 1341 and 1589 cm^{-1} are attributed to defect-related D peak and G peak, arising from vibrations of sp^2-hybridized carbon atoms,[21] while weak peaks at 2734, 2978, and 3073 cm^{-1} are attributed to 2D, D + G, and 2D′ of reduced graphene oxide, respectively.[22] Raman spectroscopy is a powerful tool not only to distinguish sp^2 and sp^3 hybridized carbon atoms, but also to discriminate single-, bi-, and few-layer graphene. It is regarded that the position of the Raman G-mode in mechanically exfoliated single-layer graphene varies from 1582 to 1594 cm^{-1}.[23] The G-mode of PTG is present at 1589 cm^{-1}, suggesting that the reduced graphene oxide nanosheets in PTG belong to single-layer graphene. Another important view for G peak in the Raman spectrum is that it will shift to lower frequencies by electron donors to higher frequencies by electron acceptors.[23] The G-peak of PTG (1589 cm^{-1}) presents about 13 cm^{-1} downshift compared with GO (1602 cm^{-1}), which is attributed to the anatase TiO_2, an n-type semiconductor, being an electron donor in PTG,[24] as well as the reduction of GO into

dx.doi.org/10.1021/ic301378j | Inorg. Chem. 2012, 51, 9544−9551

rGO. Obviously, this downshift to low frequency of G-mode in the Raman spectrum of PTG demonstrated the chemical doping of reduced graphene oxide in PTG sample. The 2D peak (2734 cm^{-1}) of PTG exhibits an upshift of 35 cm^{-1} compared to mechanical exfoliated single-layer graphene (2699 cm^{-1}),[22a] which is attributed to the changes in the phonon wavevector arising from relative movement of the Dirac cones.[25]

The composition of PTG was further studied by X-ray photoelectron spectroscopy (XPS) (Figure 4). The atomic

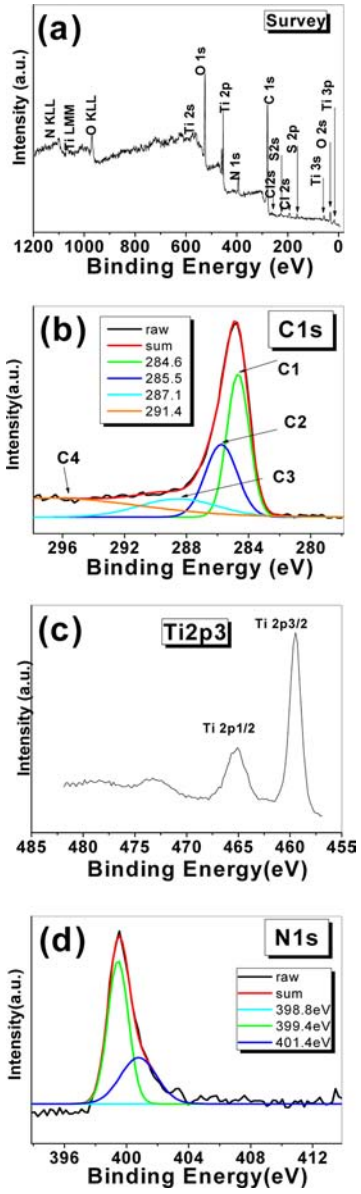

Figure 4. XPS spectrum of PTG (a) survey, (b) C1s, (c) Ti2p, and (d) N1s.

percentages are C1s 64.34%, N1s 7.21%, Ti 5.89%, and O1s 22.56%, respectively (Figure 4a). The C1s spectrum of PTG can be deconvoluted into four peaks (Figure 4b). The main peak located at a binding energy of 284.7 eV is related to the C—C bonding (sp^2 carbon, C1) in defect-free graphite, the peak at 285.8 eV is related to the C—N or C—O or C═N bonding (C2), the peak at 288.6 eV is related to the carbonylate C (HO—C═O) or C—N^+ (C3), and the peak at 296.9 eV is related to O—C═O (C4) components.[22b] The oxidation state of the Ti element in PTG is confirmed to be +4; accompanying peaks centered at 459.5 and 465.1 eV are related to Ti 2p3/2 and to Ti 2p1/2, respectively, similar to those of fully oxidized anatase TiO_2 single crystals (Figure 4c).[26] The N1s core level can be deconvoluted into three peaks (Figure 4d). The binding energies centered at 398.8 and 399.4 eV are attributed to the quinoid imine [═N—] and the benzenoid amine [—NH—], respectively. The peak at 401.4 eV is attributed to the cationic nitrogen atoms (═NH^+) in PANI.[22b]

Nitrogen isotherm adsorption/desorption curves together with the pore size distribution of PTG are shown in Figure. 5,

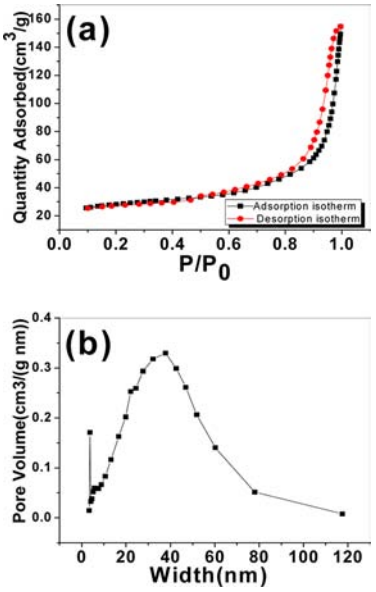

Figure 5. (a) Nitrogen adsorption/desorption isotherms demonstrate the mesoporous structure of PTG. (b) The corresponding pore size distribution.

which shows the type-IV isotherm with a H3 hysteresis loop (i.e., the adsorption isotherm is not coincident with the desorption isotherm), suggesting a characteristic of mesopores within PTG nanocomposites. The characteristic hysteresis loop of the type IV isotherm is indicative of small mesopores (Figure 5a).[27] Also, the narrow hysteresis loop during the overall pressure change suggests that the mesopores are open; thus, there is no significant delay between the capillary evaporation and condensation for N_2.[12] The Brunauer–Emmett–Teller (BET) analysis of PTG reveals a specific surface area of about 89.6 m^2/g. The pore size distribution shows a unimodal peak around 38 nm (Figure 5b). The high surface area and mesoporous structure of PTG suggest that improved electrochemical performances of anode material in lithium ion batteries can be expected.[10a]

The morphology of the PTG was characterized by transmission electron microscopy (TEM) and atomic force microscopy (AFM) images. The morphology of the compoisite material is consistent with the PANI-modified RGO sheets in the range of micrometers. The sizes of TiO_2 nanoparticles anchored on the sheets are in the range of several nanometers (Figure 6a), matched well with the XRD analysis. No unattached nanoparticles can be observed from the TEM image. The thin sheets with a thickness of 1–2 nm also can be clearly observed from AFM image (Figure 6b). The interaction

dx.doi.org/10.1021/ic301378j | Inorg. Chem. 2012, 51, 9544–9551

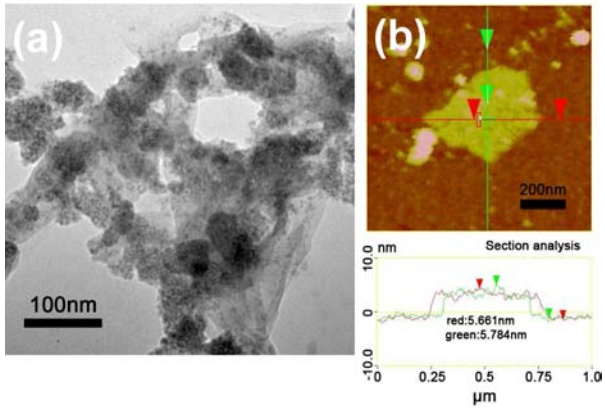

Figure 6. (a) TEM image and (b) AFM image of PTG.

among TiO_2 nanoparticles, rGO, and PANI is attributed to van der Waals forces. Even van der Waals forces (about 1 kJ/mol) are not the most significant interaction at the macroscale, but they assume huge importance at the nanoscale,[28] and van der Waals forces are favorable for enhancing the stability of the formed complex structures.

Figure 7 displays the voltage profiles of electrochemical cells made of the PTG nanocomposite at a rate of 5 C (1000 mA/g) in the voltage range 0.01−2.5 V (vs Li^+/Li). The C-rate is defined as the time in hours required to fully charge or discharge an electrode or battery. Thus, nC-rate corresponds to the full discharge in 1/n hour.[10a] The first discharge and charge steps deliver specific capacity of 496.3 and 210.9 mAh/g, respectively (Figure 7a). Interestingly, the first discharge capacity is found to 496.3 mAh/g, corresponding to a nominal insertion coefficient of $x = 1.48$. A comparable value has been observed for anatase TiO_2 hollow colloid.[29] This irreversible Li storage is attributed to the Li surface storage in the hybride graphene-based TiO_2 nanostructure.[29,30] The initial reversible capacity (i.e., second cycle) is 232.8 mAh/g. The large initial capacity reduction of the PTG electrode can be partly attributed to the reductive decomposition of electrolyte, leading to the formation of solid electrolyte interphase (SEI) layer on the electrode surface of the active material and/or from irreversible lithium insertion into nanocomposites during the first discharging step, and the storage of Li^+ in sandwichlike nanostructure of PTG, which is difficult to remove.[31] Usually, the SEI formation will lead to the generation of irreversible capacity of the anode. During the first discharge, the potential continuously drops down to 0.0099 V without any flat stage. From the second cycle onward, the shape of the voltage profiles is largely unchanged. The discharge capacities at 2nd, 5th, 10th, 20th, 50th, and 100th cycles are 232.8, 187.3, 171.7, 164.5, 160.9, and 149.8 mAh/g at a 5 C rate condition, respectively. The reversible capacity fade from the second cycle to the 100th cycle is about 0.8 mAh/g per cycle.

It is worth pointing out that the sandwiched PTG hybrid material is even better than our previously reported TiO_2 nanoparticles anchored on RGO (TGC).[2c] The first discharge and charge capacities of TGC at 5 C (1000 mA/g) are 395.3 and 169.9. mAh/g, respectively. However, the sandwiched PTG presents the first discharge and charge capacities of 496.3 and 210.9 mAh/g, about 125.6% and 124.1% in comparison with those of TGC under the same measurement conditions, with the improvement of 101 and 41 mAh/g, respectively. Also, the initial reversible capacity of 232.8 mAh/g of sandwiched PTG is

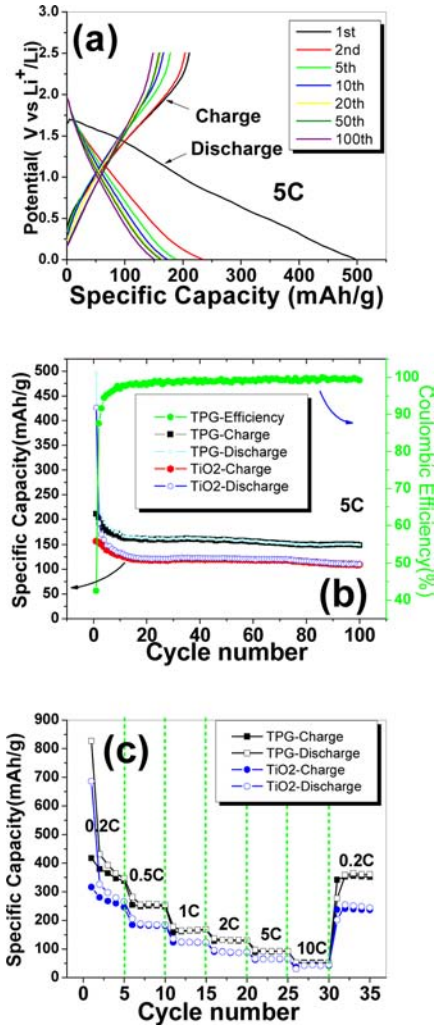

Figure 7. (a) Fast discharge/charge of PTG electrode at 5 C (1000 mA/g). (b) Cyclic performance of PTG electrode at fast rate of 5 C. (c) Variation of discharge specific capacitance of electrode at stepwise increasing rates from 0.2 C to 10 C, and then back to 0.2 C.

larger than that of TGC (199.6 mAh/g), which is about 116.6% in comparsion with that of TGC, with an increase of 33.2 mAh/g.[2c] The capacity of PTG at the 100th cycle is 149.8 mAh/g which is close that of TGC of 156.1 mAh/g, i.e., 95.96% in comparsion with that of TGC, within the range of measurement error.

In order to understand the performance of PTG nanocomposite electrode compared with pure TiO_2, we tested the cycling performance of a pure anatase TiO_2 synthesized under a similar process to that of PTG but without adding GO as well as aniline in the reaction system, under the same test conditions. Figure 7b displays the curves of charge/discharge capacity versus cycle number for PTG nanocomposite electrode, as well as TiO_2 electrode, at a rate of 5 C. After 100 cycles (5 C charge and discharge), the capacity retention of the PTG electrode is 64.3% of the value at the second cycle (i.e., initial reversible cycle) (Figure 7b). Capacity fading is ~0.698% per cycle. As is seen, both of the PTG and TiO_2 show superior cycling performance over extended cycling. It shows that PTG starts at 496.3 mAh/g and still maintains at 149.8 mAh/g after 100 cycles, with a capacity loss of 69.8%, while the capacity of TiO_2 starts at 426.4 mAh/g and maintains at 110.3 mAh/g after 100 cycles with a capacity loss of 74.1%.

dx.doi.org/10.1021/ic301378j | Inorg. Chem. 2012, 51, 9544−9551

Obviously, compared with pure TiO_2, the specific capacity of PTG after 100th cycle (149.8 mAh/g) was 1.35 times of that pure TiO_2 (110.3 mAh/g), even at such a high charge/discharge rate of 5 C (1000 mA/g) (Figure 7b). This experiment result suggests that PTG provides enhancement in electrically connected channels and embedded TiO_2 supporting layers.[32] The initial reversible capacity (second cycle) of TiO_2 (192.2 mAh/g) is only amounting to 82.6% of that of PTG (232.8 mAh/g), while the reversible capacity after 100 cycles of TiO_2 is only amounting to 73.6% of that of PTG, suggesting that the doped rGO and PANI in PTG indeed function with an enhanced effect compared with TiO_2, not only the capacity but also the cycling ability. Furthermore, the Coulombic efficiency of PTG stays steadily above 95% since the fifth cycle, keeps an increasing trend in the following process of recharging, and reaches 99.19%, close to 100%, at the 100th cycle, which suggests the large promotion of reaction reversibility of lithium intercalation/deinsertion in PTG. The improved cycleability of the PTG electrode is based on its specific sandwich-like mesoporous nanostructure, that provides the following advantages: (i) The sandwiched structure of PTG offers adequate void space to "storage" lithium.[33] (ii) The TiO_2 nanoparticles embedded among graphene nanosheets and PANI particles as well as PNAI itself provide higher specific surface areas, which improve the electrical contact as well as lithium ion conduction.

Figure 7c shows the rate capability of PTG electrode: it delivers averaged rate capacity of about 472.44 mAh/g at 0.2 C, 260.56 mAh/g at 0.5 C, 168.24 mAh/g at 1 C, 131.74 mAh/g at 2 C, 93.08 mAh/g at 5 C, 51.12 mAh/g at 10 C, and 344.24 mAh/g when returning to 0.2 C again, respectively; pure TiO_2 electrode delivers averaged rate capacity of about 370.52 mAh/g at 0.2 C, 189.50 mAh/g at 0.5 C, 125.82 mAh/g at 1 C, 89.82 mAh/g at 2 C, 64.84 mAh/g at 5 C, 40.56 mAh/g at 10 C, and 239.52 mAh/g when returning to 0.2 C again, respectively. When cycled for PTG at 0.2 C again after the sample with an averaged capacity of 344.34 mAh/g was tested for five cycles at each rate ranging from 0.2 C to 10 C, about 72.86% of the initial averaged capacity of 472. 44 mAh/g at 0.2 C was recovered; however, only 64.64% capacity of initial averaged capacity was recovered for pure TiO_2 at the same processes, confirming that structural stability of PTG is better than that of TiO_2 (Figure 7c). Furthermore, the averaged capacity of PTG (344.24 mAh/g) when it returns to 0.2 C again is 1.43 times of that of pure TiO_2 (239.52 mAh/g). This experiment further demonstrates that PTG provides enhancement in electrically connected channels and embedded TiO_2 supporting layers.[32]

It is worth pointing out that the rate capacity of PTG is also better than that of our previously reported TGC.[2c] The averaged rate capacity of about 472.44 mAh/g at 0.2 C and 344.24 mAh/g when it returns back to 0.2 C again is larger than those of TGC of 295.9 and 266.7 mAh/g, correspondingly, which are 137.2% and 129.1% in comparison with those of TGC under the same measurement conditions, with the improvement of 176.54 and 77.54 mAh/g, respectively. These data demonstrated that the sandwiched PTG presented distinct improvement of rate performance. It is known that rapid ionic and electronic transport is necessary for achieving a high rate capacity of LIBs. Obviously, the improvement can be attributed to the sandwiched structure which is different from that of TGC. The structural stability of PTG can be attributed to the concept of sandwich-like structure of PTG. The good charge/discharge rate performance of LIBs can be attributed to the conducting polymer PANI and graphene sheets in PTG nanocomposites, due to the corresponding good transport of Li^+ ions and/or electrodes. The improved electrochemical performance of PTG electrode is probably due to its sandwiched mesoporous structure, ensuring a high electrode–electrolyte contact area, as well as providing storage of the extra amount of lithium.[34] Moreover, the TiO_2 particles in PTG shorten the transport lengths for both lithium ions and electron; the conducting polymer PANI is favorable to fast discharge and charge.

The results of Figure 7 confirm the expectation of fast and high-capacity delivery and of long cycling stability in our PTG nanocomposite electrode. The fast high-capacity retention is a clear indication that the mechanical integrity of the electrode is fully maintained. The results indicate that the improvement in electrochemical performance, in terms of cycling performance and rate performance, should not only be attributed to the TiO_2 nanoparticles themselves, but also to the sandwich-like structure of PTG composed of effective carbon matrix, i.e., graphene nanosheets and conducting polymer PANI. It has been demonstrated that general approaches for enhancing ion and electron transport kinetics in batteries include designing electrode materials with high ion diffusion constants and coating electrolytically active material with a conductive layer.[2a] Reducing the dimensions of active materials is an effective method in improving battery cycling rates, due to nanoscale electrodes having exceptionally short ion and electron transport lengths, which would reduce the lithium ion and electron diffusion time.[35] In fact, a three-dimensional interpenetrating network is suggested as ideal electrode architecture for providing efficient lithium ion and electron transport.[2a] It is known that there are some advantages for nanoparticles used as electrodes in LIBs, such as shortening diffusion path lengths for electrons and lithium ions, which is favorable for rapid solid-state Li^+ and electron transport.[1b] However, the disadvantages of nanoparticles used as electrodes in LIBs include inferior packing of particles, leading to lower volumetric energy densities.[36] So, it is very important to avoid the nanoparticle aggregation during the charge/discharge processes. Carbonaceous materials are very stable anode materials in LIBs, due to the small volume change during Li insertion/extraction.[37] Therefore, the rGO and PANI sandwich-like PTG nanostructures (i.e., TiO_2 nanoparticles sandwiched between carbonaceous rGO and PANI sheets) used for anode material in LIBs (rGO and PANI) may serve as perfect barriers to protect the interlayered (or sandwiched) active TiO_2 and maintain its high capacity. The particular sandwiched structure can function as barrier layers and prevent the aggregation of TiO_2 nanoparticles. A similar function of carbonaceous barriers (such as carbon coatings) has been reported.[10b,37,38] So, we can say that sandwiched PTG hybrid material can not only avoid the TiO_2 nanoparticles aggregation upon cycling, but also facilitate the fast migration of Li^+ ions and electrons.

The electrochemical properties of PTG and pure TiO_2 were further studied by measuring their cyclic votammetry (CV) curves using a three-electrode symmetric system (i.e., the same materials are used as both cathode and anode) under different scan rates varying from 5 to 100 mV/s between −0.1 and 0.4 V (Figure S2). Obviously, the specific capacitance for the PTG of 228.8, 181.6, 93.12, and 64.72 F/g obtained at 5, 10, 50, and 100 mV/s in 6 M KOH aqueous solution are markedly larger than those of pure TiO_2 of 3.92, 3.76, 3.36, 3.2 F/g at the same measurement condition, respectively, suggesting good capaci-

dx.doi.org/10.1021/ic301378j | Inorg. Chem. 2012, 51, 9544–9551

tive behavior, rapid diffusion of electrolyte ions from the solution into the pores of the PTG, and low equivalent series resistance (ESR) of the PTG electrode compared with that in pure TiO_2 electrode.

The main goal of this work was the development of a concept for constructing electrode configuration favorable to fast charge/discharge rates for LIBs electrodes. The approach for embedding nanostructured TiO_2 among conducting polymer PANI and graphene sheets as anode in LIBs demonstrates that fast charge/discharge rate accompanying long life can be achieved.

In comparison, Qiu et al. reported anatase TiO_2@TiO_xN_y/TiN-graphene nanocomposites display an initial discharge capacity of ~314 mAh/g at C/5 (i.e., 33.6 mAh/g), 175 mAh/g at C/3 (i.e., 56 mA/g), 166 mAh/g at 1 C (1 C = 168 mA/g), 150 mAh/g at 3 C (i.e., 504 mA/g), 130 mAh/g at 12 C (i.e., 2016 mA/g), and finally resumed ~165 mAh/g when the rate was reduced back to C/3, respectively.[39] Ye et al. reported anatase mesocrystal electrode displayed a discharge capacity of 204.7 mAh/g in the first cycle, and about 151.6 mAh/g (74.2% of initial discharge capacity) after 60 cycles at a current density of 1 C (=170 mA/g).[40] Lou et al. reported anatase TiO_2 hollow particles used in LIBs exhibit the first discharge capacity of 408 mAh/g, and deliver a capacity of 112 mAh/g at a high rate of 2 C (670 mA/g),[29] and our previously reported TGC[2c] exhibits the first discharge capacity of 395.3 mAh/g, and delivers a capacity of 144.7 mAh/g at a high rate of 2 C, 121.7 mAh/g at 5 C (1000 mA/g), while the PTG nanocomposites exhibit the first discharge capacity of 496.3 mAh/g and deliver a capacity of 149.8 mAh/g at an even higher rate of 5 C (1000 mA/g) condition. All these data demonstrated that the sandwiched PTG hybrid nanostructures indeed exhibit some improvement of anode perfromance.

4. CONCLUSIONS

In summary, we have developed a novel and simple method to synthesize TiO_2-based sandwichlike PTG nanocomposites. As a result, the PANI-TiO_2-rGO nanocomposite is a promising anode material for highly efficient LIBs with fast charge/discharge rate and highly enhanced cycling performance [discharge capacity of 149.8 mAh/g accompanying Coulombic efficiency of 99.19% at a current density of 5 C (1000 mA/g) after 100 cycles] which exhibits enhanced electrochemical performance over pure TiO_2. We can conclude that the concept of applying complex TiO_2-based nanocomposite as electrode in LIBs may open a new area of research for the development of practical transition-metal oxide-based electrodes and will be important to the progress of the LIB science and technology.

■ ASSOCIATED CONTENT

Supporting Information

TEM image and cyclic voltammogram (CV) curves of PTG and pure TiO_2 at different rates. This material is available free of charge via the Internet at http://pubs.acs.org.

■ AUTHOR INFORMATION

Corresponding Author

*E-mail: yuedm@mail.buct.edu.cn (D.Y.), hqcao@mail.tsinghua.edu.cn (H.C.).

Notes

The authors declare no competing financial interest.

■ ACKNOWLEDGMENTS

The authors acknowledge financial supports from the National Natural Science Foundation of China (20921001).

■ REFERENCES

(1) (a) Tarascon, J.-M.; Armand, M. *Nature* **2001**, *414*, 359. (b) Armand, M.; Tarascon, J.-M. *Nature* **2008**, *451*, 652. (c) Dunn, B.; Kamath, H.; Tarascon, J.-M. *Science* **2011**, *334*, 928.

(2) (a) Zhang, H.; Yu, X.; Braun, P. V. *Nat. Nanotechnol.* **2011**, *6*, 277. (b) Kang, B.; Ceder, G. *Nature* **2009**, *458*, 190. (c) Cao, H.; Li, B.; Zhang, J.; Lian, F.; Kong, X.; Qu, M. *J. Mater. Chem.* **2012**, DOI: 10.1039/c2jm0007e.

(3) Kovalenko, I.; Zdyrko, B.; Magasinski, A.; Hertzberg, B.; Milicev, Z.; Burtovyy, R.; Luzinov, I.; Yushin, G. *Science* **2011**, *334*, 75.

(4) McFarland, E. W.; Tang, J. *Nature* **2003**, *421*, 616.

(5) Tisdale, W. A.; Williams, K. J.; Timp, B. A.; Norris, D. J.; Aydil, E. S.; Zhu, X.-Y. *Science* **2010**, *328*, 1543.

(6) Green, I. Xi.; Tang, W.; Neurock, M.; Yates, J. T. *Science* **2011**, *333*, 736.

(7) Wagemaker, M.; Kentgens, A. P. M.; Mulder, F. M. *Nature* **2002**, *418*, 397.

(8) Hu, Y.-S.; Kienle, L.; Guo, Y.-G.; Maier, J. *Adv. Mater.* **2006**, *18*, 1421.

(9) Wan, M. *Conducting Polymers with Micro or Nanometer Structure*; Tsinghua University Press-Springer: Beijing, China, 2008.

(10) (a) Li, B.; Cao, H.; Shao, J.; Qu, M. *Chem. Commun.* **2011**, *47*, 10374. (b) Li, B.; Cao, H.; Shao, J.; Qu, M.; Warner, J. H. *J. Mater. Chem.* **2011**, *21*, 5069. (c) Li, B.; Cao, H.; Shao, J.; Li, G.; Qu, M.; Yin, G. *Inorg. Chem.* **2011**, *50*, 1628. (d) Li, B.; Cao, H.; Zhang, J.; Qu, M.; Lian, F.; Kong, X. *J. Mater. Chem.* **2012**, *22*, 2851. (e) Liang, R.; Cao, H.; Qian, D.; Zhang, J.; Qu, M. *J. Mater. Chem.* **2011**, *21*, 17654.

(11) (a) Chiang, Y. M. *Science* **2010**, *330*, 1485. (b) Huang, J. Y.; Zhong, L.; Wang, C. M.; Sullivan, J. P.; Xu, W.; Zhang, L. Q.; Mao, S. X.; Hudak, N. S.; Liu, X. H.; Subramanian, A.; Fan, H.; Qi, L.; Kushima, A.; Li, J. *Science* **2010**, *330*, 1515. (c) Lou, X. W.; Li, C. M.; Archer, L. A. *Adv. Mater.* **2009**, *21*, 2536.

(12) Yang, S.; Feng, X.; MüLlen, K. *Adv. Mater.* **2011**, *23*, 3575.

(13) *The Principle and Applications of X-ray Diffraction Analysis*; Liu, E.-H., Liu, P. A., Eds.; Chemical Industry Press: Beijing, China, 2003.

(14) Chen, X.; Lou, Y.; Samia, A. C. S.; Burda, C.; Gole, J. L. *Adv. Funct. Mater.* **2005**, *15*, 41.

(15) Williams, D. H.; Fleming, I. *Spectroscopic Methods in Organic Chemistry*, 6th ed.; McGraw-Hill Companies, Inc.: London, U.K., 2008.

(16) *Modern Organic Spectrum Analysis*; Zhang, H., Peng, Q., Li, Y., Zhang, R., Eds.; Chemical Industry Press: Beijing, China, 2005.

(17) Liu, C.; Sun, H.; Yang, S. *Chem.—Eur. J.* **2010**, *16*, 4381.

(18) Woggon, U. *Optical Properties of Semiconductor Quantum Dots*; Springer: Berlin, 1997.

(19) (a) Arora, A. K.; Rajalakshmi, M.; Ravindran, T. R.; Sivasubramanian, V. *J. Raman Spectrosc.* **2007**, *38*, 604. (b) Arora, A. K.; Rajalakshmi, M.; Ravindran, T. R. *Encyclopedia of Nanoscience and Nanotechnology*; Nalwa, N. S., Ed.; American Scientific Publishers: Los Angeles, CA, 2004; Vol. *8*.

(20) Yan, Y.; Fang, J.; Zhang, Y.; Fan, H.; Wei, Z. *Macromol. Rapid Commun.* **2011**, *32*, 1640.

(21) Elias, D. C.; Nair, R. R.; Mohiuddin, T. M. G.; Morozov, S. V.; Blake, P.; Halsall, M. P.; Ferrari, A. C.; Boukhvalov, D. W.; Katsnelson, M. I.; Geim, A. K.; Novoselov, K. S. *Science* **2009**, *323*, 610.

(22) (a) Rao, C. N. R.; Sood, A. K.; Subrahmanyam, K. S.; Govindaraj, A. *Angew. Chem., Int. Ed.* **2009**, *48*, 7752. (b) Liang, R.; Cao, H.; Qian, D.; Zhang, J.; Qu, M. *J. Mater. Chem.* **2011**, *21*, 17654.

(23) Rao, A. M.; Eklund, P. C.; Bandow, S.; Thess, A.; Smalley, R. E. *Nature* **1997**, *388*, 257.

(24) Kumarasinghe, A. R.; Flavell, W. R.; Thomas, A. G.; Thomas, A. K.; Mallick, A. K.; Tsoutsou, D.; Chatwin, C.; Rayner, S.; Kirkham, P.; Warren, S.; Patel, S.; Christian, P.; O'Brien, P.; Grätzel, M.; Hengerer, R. *J. Chem. Phys.* **2007**, *127*, 114703.

(25) Mohiuddin, T. M. G.; Lombardo, A.; Nair, R. R.; Bonetti, A.; Savini, G.; Jalil, R.; Bonini, N.; Basko, D. M.; Galiotis, C.; Marzari, N.; Novoselov, K. S.; Geim, A. K.; Ferrari, A. C. *Phys. Rev. B* **2009**, *79*, 205433.
(26) Yang, H. G.; Sun, C. H.; Qiao, S. Z.; Zou, J.; Liu, G.; Smith, S. C.; Cheng, H. M.; Lu, G. Q. *Nature* **2008**, *453*, 638.
(27) Erbil, H. Y. *Surface Chemistry of Solid and Liquid Interfaces*; Blackwell Publishing: Oxford, U.K., 2006.
(28) Hornyak, G. L.; Dutta, J.; Tibbals, H. F.; Rao, A. K. *Introduction to Nanoscience*; CRC Press: Boca Raton, FL, 2008.
(29) Lou, X. W.; Archer, L. A. *Adv. Mater.* **2008**, *20*, 1853.
(30) Guo, Y.-G.; Hu, Y.-S.; Maier, J. *Chem. Commun.* **2006**, 2783.
(31) (a) Yu, Y.; Gu, L.; Wang, C.; Dhanabalan, A.; van Aken, P. A.; Maier, J. *Angew. Chem., Int. Ed.* **2009**, *48*, 6485. (b) *Principle and Key Technology of Lithium Ion Battery*; Huang, K., Wang, Z., Liu, S., Eds.; Chemical Industry Press: Beijing, China, 2007.
(32) Park, W., II; Lee, C.-H.; Lee, J. M.; Kim, N.-J.; Yi, G.-C. *Nanoscale* **2011**, *3*, 3522.
(33) Ren, Y.; Hardwick, L. J.; Bruce, P. G. *Angew. Chem., Int. Ed.* **2010**, *49*, 2570.
(34) Lou, X. W.; Wang, Y.; Yuan, X.; Lee, J. Y.; Archer, L. A. *Adv. Mater.* **2006**, *18*, 2325.
(35) (a) Lee, S. W.; Yabuuchi, N.; Gallant, B. M.; Chen, S.; Kim, B.-S.; Hammond, P. T.; Shao-Horn, Y. *Nat. Nanotechnol.* **2010**, *5*, 531. (b) Kang, B.; Ceder, G. *Nature* **2009**, *458*, 190. (c) Balke, N.; Jesse, S.; Morozovska, A. N.; Eliseev, E.; Chung, D. W.; Kim, Y.; Adamczyk, L.; García, R. E.; Dudney, N.; Kalinin, S. V. *Nat. Nanotechnol.* **2010**, *5*, 749. (d) Yang, B.; Ceder, G. *Nature* **2009**, *458*, 190.
(36) Aricò, A. S.; Bruce, P.; Scrosati, B.; Tarscon, J.-M.; Schalkwijk, W. V. *Nat. Mater.* **2005**, *4*, 366.
(37) Zhang, W.-M.; Wu, X.-L.; Hu, J.-S.; Guo, Y.-G.; Wan, L.-J. *Adv. Funct. Mater.* **2008**, *18*, 3941.
(38) Zhang, W.-M.; Hu, J.-S.; Guo, Y.-G.; Zheng, S.-F.; Zhong, L.-S.; Song, W.-G.; Wan, L.-J. *Adv. Mater.* **2008**, *20*, 1160.
(39) Qiu, Y.; Yan, K.; Yang, S.; Jin, L.; Deng, H.; Li, W. *ACS Nano* **2010**, *4*, 6515.
(40) Ye, J.; Liu, W.; Cai, J.; Chen, S.; Zhao, X.; Zhou, H.; Qi, L. *J. Am. Chem. Soc.* **2011**, *133*, 933.